PKCα: a versatile key for decoding the cellular calcium toolkit

Gregor Reither,[1] Michael Schaefer,[2] and Peter Lipp[1]

[1]Institute for Molecular Cell Biology, Medical Faculty of the Saarland University, D-66421 Homburg/Saar, Germany
[2]Institute for Pharmacology, Campus Benjamin Franklin, Charité-Universitätsmedizin Berlin, 14195 Berlin, Germany

Conventional protein kinases C (cPKCs) play an essential role in signal transduction and are believed to integrate both global Ca^{2+} transients and diacylglycerol signals. We provide evidence that PKCα is a ubiquitous readout sensor for the cellular Ca^{2+} toolkit, including highly restricted elementary Ca^{2+} release.

Threshold stimulations of cells with Ca^{2+}-mobilizing agonists resulted in PKCα translocation events with limited spatial spreads (<4 μm) comprising two groups of lifetimes; brief events (400–1,500 ms) exclusively mediated by Ca^{2+}–C2 domain membrane interactions and long-lasting events (>4 s) resulting from longer DAG-C1a domain–mediated membrane interactions.

Although upon uncaging NP-EGTA, which is a caged Ca^{2+} compound, WT-PKCα displayed rapid membrane translocations within <250 ms, PKCα constructs with C2 domains mutated in their Ca^{2+}-binding region lacked any Ca^{2+}-dependent translocation. Flash photolysis of diazo-2, a photosensitive caged Ca^{2+} buffer, revealed a biphasic membrane dissociation (slow and fast period) of WT-PKCα. The slow phase was absent in cells expressing PKCα-constructs containing mutated C1a-domains with largely reduced DAG binding. Thus, two groups of PKCα membrane interactions coexist; C2- and C1a-mediated interactions with different lifetimes but rapid interconversion.

We conclude that PKCα can readout very fast and, spatially and temporally, very complex cellular Ca^{2+} signals. Therefore, cPKCs are important transducers for the ubiquitous cellular Ca^{2+} signaling toolkit.

Introduction

Ca^{2+} is a versatile and ubiquitous messenger in all living cells. Increases in the intracellular Ca^{2+} concentration occur as long-lasting global oscillations, such as those that occur during clonal selection of white blood cells. In contrast, Ca^{2+} increases also occur as transients with a very short lifetime and high spatial confinement, so-called elementary Ca^{2+} signals (Berridge, 2002; Berridge et al., 2003). All Ca^{2+} signals require proteins to relay the Ca^{2+} concentration downstream to different signaling networks. These specialized sensors contain Ca^{2+}-binding domains and include such ubiquitous proteins as calmodulin, the structure of which comprises four highly conserved binding domains, the so-called EF hands (Vetter and Leclerc, 2003). Another very important Ca^{2+}-binding domain is the C2 domain; e.g., during synaptic signaling, where it functions as the Ca^{2+}-sensing domain of Munc-13 (Rettig and Neher, 2002). A subfamily of the PKCs, the conventional PKCs (cPKCs), also contain C2 domains and, hence, have the principle ability to decode cellular Ca^{2+} transients (Kohout et al., 2002). This family belongs to the AGC kinases (Manning et al., 2002) and comprises 12 isoforms, which are distinguished depending on their sensitivity toward signaling molecules.

The intrinsic function of PKC isozymes is regulated by multiple mechanisms (Newton, 2001), and they decode a variety of stimulation-induced intracellular messengers (Oancea and Meyer, 1998). PKCs are believed to translate messengers into the phosphorylation of many target proteins, such as ion transporters (e.g., Na^+/Ca^{2+} and Na^+/H^+ exchangers; Philipson and Nicoll, 2000; Avkiran and Haworth, 2003) and proteins involved in the control of cell growth and proliferation (e.g., MAPK, Ras, and Raf; Nishikawa et al., 1997; Clerk and Sugden, 2001).

Phosphorylation assays with target proteins provide one possible way to detect PKC activity, but these approaches might be complicated by the fact that many signaling events occur only in confined subcellular spaces, the so-called signaling microdomains, and/or display a brief lifetime. Another approach

Correspondence to Peter Lipp: peter.lipp@uniklinikum-saarland.de

Abbreviations used in this paper: cPKC, conventional PKC; DAG, diacylglycerol; HEK, human embryonic kidney; LTE, local translocation event; PIP_2, phosphatidyl-4,5-bisphosphate; PMA, phorbol 12-myristate 13-acetate; PS, phosphatidylserine; ROI, region of interest; WT, wild-type.

The online version of this article contains supplemental material.

The Journal of Cell Biology, Vol. 174, No. 4, August 14, 2006 521–533
http://www.jcb.org/cgi/doi/10.1083/jcb.200604033

is to follow translocation events in cells. Most of these experiments were performed by using long-lasting stimuli such as fatty acids (Shirai et al., 1998) or phorbolesters (e.g., phorbol 12-myristate 13-acetate [PMA]; Braz et al., 2002). These methods were typically combined with an in vitro readout at predefined time points during the stimulation process; thus, interpretation at the single-cell level was complicated by cell–cell variability and limited temporal resolution.

In contrast, real-time live-cell imaging overcomes many of these drawbacks. For this, fluorescent proteins of various colors are coupled to the C termini of PKCs, and translocation is followed by video or confocal imaging (Mogami et al., 2003). With such an approach, Schaefer et al. (2001) presented evidence for diffusion-limited fast translocation kinetics of PKCα in histamine receptor–overexpressing human embryonic kidney (HEK) 293 cells (Lenz et al., 2002). To follow these events with appropriate temporal resolution, these authors used confocal linescanning by sacrificing one spatial dimension for a gain in acquisition speed. In contrast, Codazzi et al. (2001) used total internal reflection microscopy imaging and found fast and robust responses of the neuronal cPKCγ. In addition, they could provide some initial evidence for spatially more complex translocation events, but these studies were restricted by their limited temporal resolution of several seconds per image and their confinement to PKC measurements at the plasma membrane level.

We have used 2D real-time confocal microscopy of fluorescent PKCα fusion constructs in two cell types to comprehensively characterize cPKC translocation dynamics. The α-isoform was chosen because it is the most ubiquitously expressed PKC isoform and, in contrast to other ubiquitous cPKCs (e.g., PKCβ),

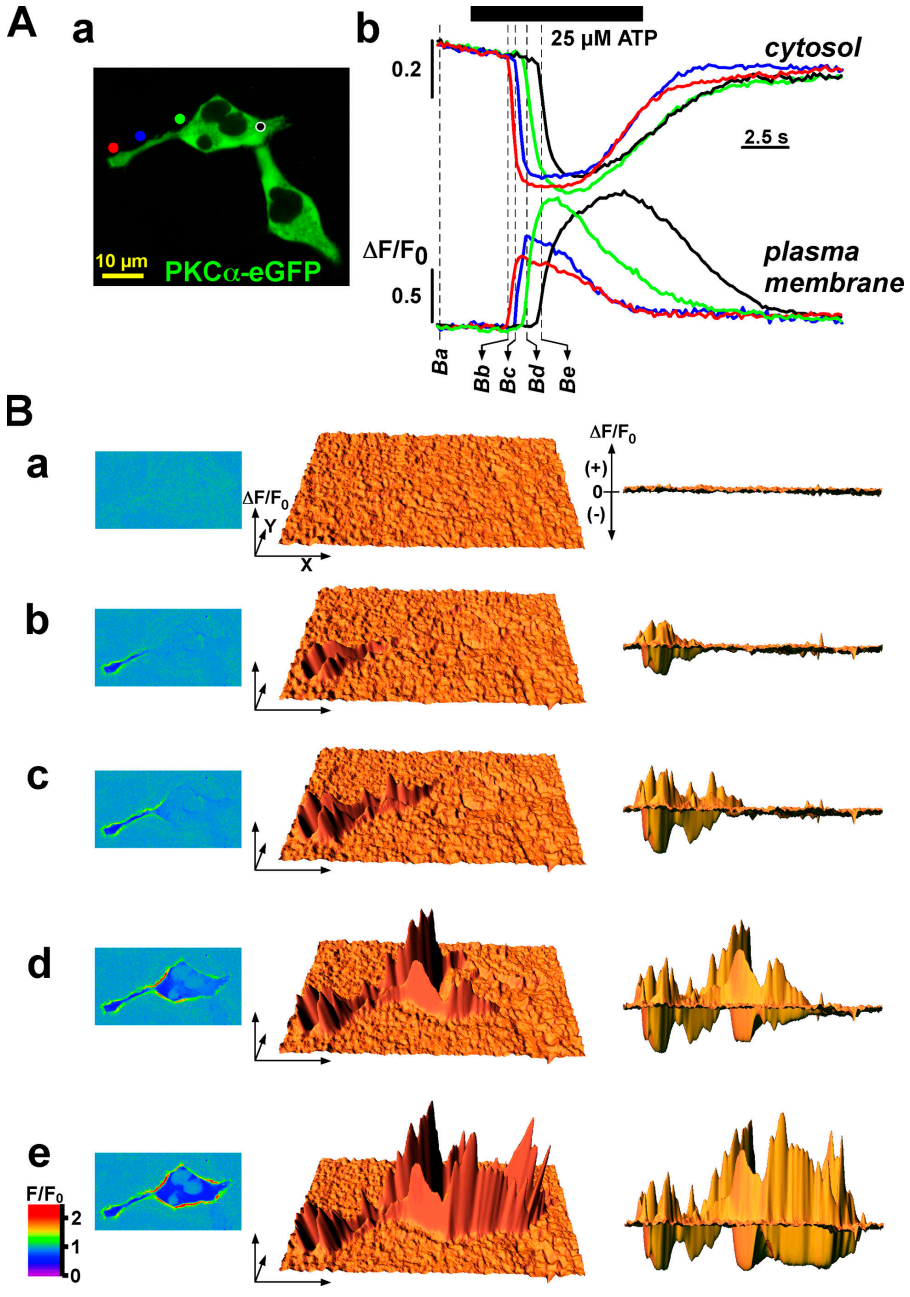

Figure 1. **PKCα translocation waves.** HEK293 cells were transfected with PKCα-EGFP and stimulated with ATP. (A, a) Cells expressing the PKCα construct. The colored circles mark cellular locations from which fluorescence was averaged for the corresponding fluorescence tracings in A (b). For those time points marked with the vertical dashed lines, individual confocal images have been analyzed in B. The labels in A (b) correspond to B (a–e). For the left column in B, we calculated the relative fluorescence and color coded the ratio according to the color wedge in B (e). 3D surface plots of the relative fluorescence have been constructed for the middle and right columns, which represent two different viewing angles onto the same surface. Upward deflections indicate relative increases and downward deflections indicate relative decreases in the local PKCα-EGFP concentration. Similar results were obtained in 15 additional cells from 10 independent experiments.

there is only a single variant (Kofler et al., 2002). We particularly concentrated on the question of whether and to what degree cPKCα can decode the spatially and temporally very complex Ca^{2+} transients that occur during physiological Ca^{2+} signaling in living cells (Berridge et al., 2003) into translocation signals and on PKCα membrane interactions via their C2 and C1 domains.

Results

Physiologically, PKCα is stimulated by diacylglycerol (DAG) through binding to its C1a domain (Medkova and Cho, 1999), which is produced, e.g., as a product of PLCβ-mediated hydrolysis of phosphatidyl-4,5-bisphosphate (PIP_2), and by Ca^{2+} through its C2 domains. To activate these signaling networks, we used ATP stimulation of HEK293 and COS1 cells because they endogenously express P2Y receptors that couple to G_q proteins. In the vast majority of cells stimulated with robust agonist concentrations, we found global oscillations of both Ca^{2+} and PKCα-EYFP (Fig. S1, available at http://www.jcb.org/cgi/content/full/jcb.200604033/DC1), and variations of the agonist concentration were readily translated into graded Ca^{2+} signals and PKCα-EGFP translocations (Fig. S1 and Video 1).

Stimulation of cells with lower concentrations of Ca^{2+}-mobilizing agonists often leads to Ca^{2+} transients with complex spatiotemporal properties, such as waves or spatially restricted Ca^{2+} responses (for review see Berridge et al., 2000). Thus, we questioned to what degree PKCα is able to decode the complexity of Ca^{2+} signals into translocation events. Fig. 1 depicts an analysis of the translocation process evoked by a Ca^{2+} wave using rapid 2D confocal imaging. Regularly, linescans or slow 2D image acquisition can produce data that are difficult to interpret (Bootman et al., 1997a). The Ca^{2+} wave underlying the response shown in Fig. 1 brought about a wave-like translocation of PKCα-EGFP that can be seen in the pseudocolored self-ratio images (Fig. 1 B, left column). To selectively depict the spatial properties of such translocation waves on the whole-cell level, we have plotted the relative fluorescence changes as increases or decreases in the height of 3D surface for the entire 2D plane (Fig. 1 B, middle and right columns; and Video 2, available at http://www.jcb.org/cgi/content/full/jcb.200604033/DC1). From such data, we concluded that PKCα is able to reliably decode even fast Ca^{2+} waves propagating through cells into translocation waves.

Low agonist concentrations provoke spatially complex Ca^{2+} signals (Berridge et al., 2000). The investigation of subcellular

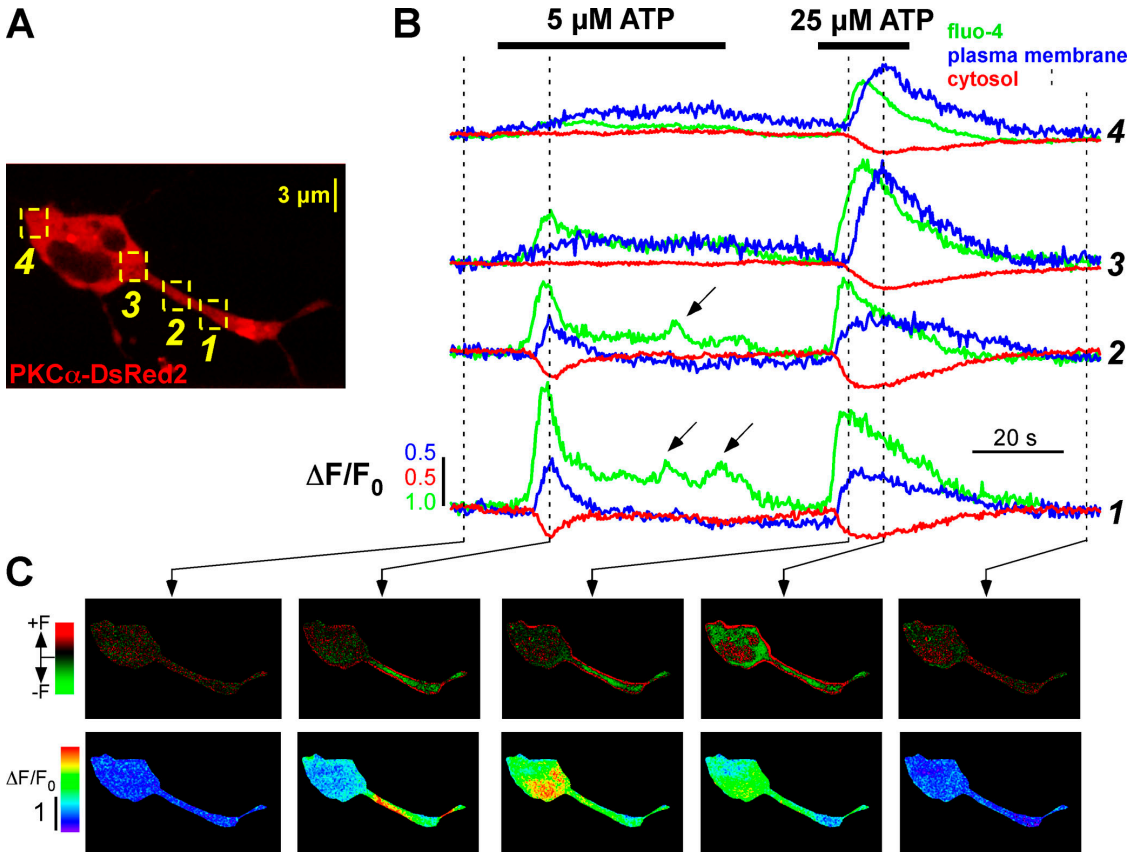

Figure 2. **Spatially restricted Ca^{2+} signals induced spatially confined PKCα translocations.** HEK293 cells were transfected with PKCα-DsRed2 and loaded with fluo-4. (A) The cellular regions used for the analysis in B. The stimulation regime is indicated by the horizontal bars in B. The green traces in B show the time course of the relative fluo-4 fluorescence, and the blue and red tracings represent PKCα-DsRed2 fluorescence at the plasma membrane and in the adjacent cytosol, respectively. (C) Relative PKCα distributions (top) and relative fluo-4 signals (bottom) for the time points indicated in B. Both representations were color coded according to the color wedges to their left. Similar results were obtained in nine additional cells stimulated with the same stimulation regime.

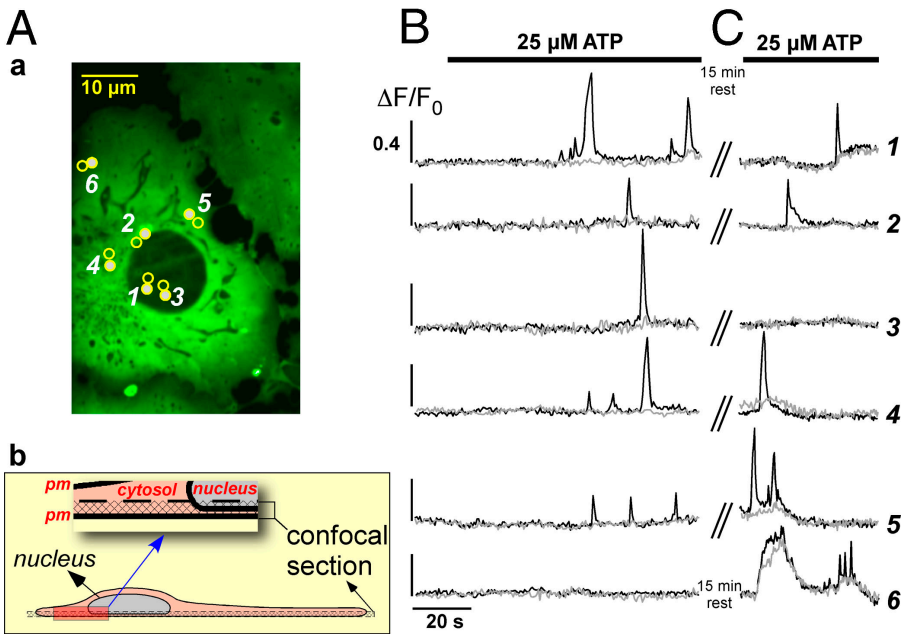

Figure 3. **Repetitive LTEs in PKCα-EYFP–expressing COS1 cells.** Cells were stimulated with ATP, as indicated in B and C. (A, a) A confocal image of a group of unstimulated COS1 cells. (A, b) The Z location of the confocal plane that was positioned close to the bottom plasma membrane. pm, plasma membrane. (B) Tracings of relative PKCα-EYFP fluorescence changes for six representative LTE locations during the initial ATP stimulation. The fluorescence of such locations (marked with open circles in A, a) has been redrawn in black. Fluorescence readings from directly adjacent locations (marked with filled circles in A) have been replotted in B in light gray. (C) Traces of the same locations as in B restimulated after 15 min of washing with an ATP-free solution. Similar data were obtained in 24 additional cells displaying a total of 70 LTE sites.

Ca^{2+} signals requires Ca^{2+} indicators with a good signal-to-noise ratio, especially for small and spatially confined Ca^{2+} signals (Thomas et al., 2000a). In PKCα-DsRed2–expressing HEK293 cells, we analyzed responses to the application of different lower ATP concentrations to provoke such Ca^{2+} signals. Fig. 2 depicts the result of such a representative experiment. Four regions of interest (ROIs; Fig. 2 A) have been analyzed, and the time courses of the normalized fluo-4 (green), plasma membrane (blue), and cytosolic (red) fluorescence of the DsRed2 constructs have been replotted in Fig. 2 B. Application of 5 µM ATP caused a Ca^{2+} signal that was largely restricted to the lower extension of the cell (Fig. 2 B, compare traces 1 and 4). The subcellular distribution of this Ca^{2+} transient can be seen in the self-ratio image displayed in Fig. 2 C (second column). Despite the fact that this Ca^{2+} signal was brief and spatially restricted, the PKCα translocation reflected that spatiotemporal property (compare traces in Fig. 2 B with the corresponding images in C). A detailed analysis of the fluo-4 fluorescence and the plasma membrane PKCα-DsRed2 fluorescence revealed a small difference between the time courses in that the fluo-4 fluorescence increase preceded the increase in the plasma membrane PKCα-DsRed2 signal by ~800 ms (i.e., four image pairs at a 5-Hz acquisition rate; in all nine experiments with the same stimulation regime the differences were always between three and four images at 5 Hz). In addition, we observed multiple

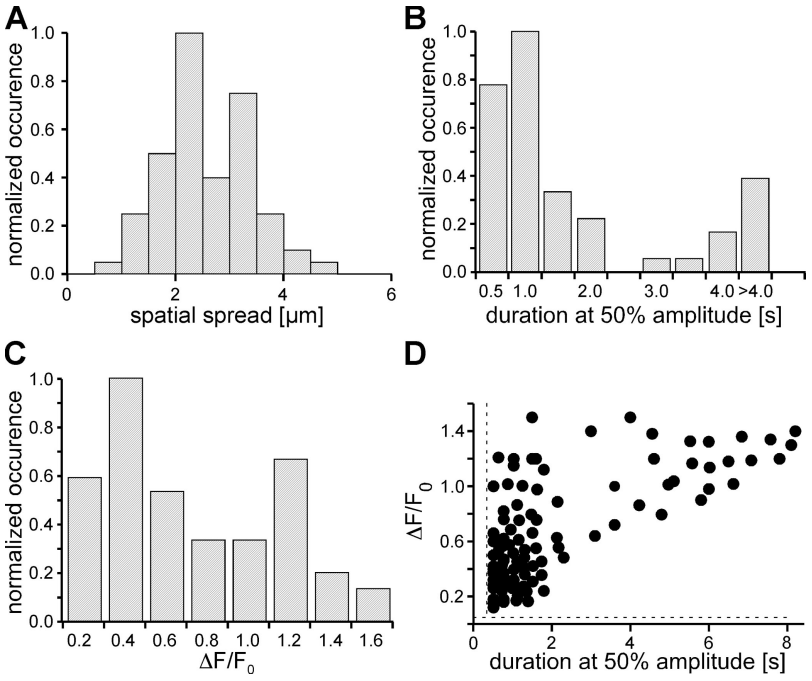

Figure 4. **Properties of LTEs in COS1 cells.** Cells were transfected either with PKCα-EYFP or -EGFP and stimulated with 25 µM ATP. (A) The distribution of the spatial spread at peak amplitude normalized to the maximal value. Fitting this dataset with a single Gauss distribution resulted in a significantly higher χ^2 than fitting with two Gauss distribution centered at ~2.2 and ~3.2 µm. For B, we measured the signal duration at 50% of their maximal amplitude and constructed the distribution by binning the data into 0.5-s time bins. Because some of these LTEs displayed very long durations, well exceeding 4 s, we combined them into one bin (>4 s). (C) The amplitudes of the LTEs were calculated as relative fluorescence changes after background subtraction normalized to the average of at least five resting images. In D, we plotted the relative amplitude of each LTE against its duration at 50% maximal amplitude. The two dashed lines depict the boundary conditions for LTEs.

small local Ca^{2+} fluctuations after the initial spike (Fig. 2 B, traces 1 and 2, arrows) that were not reflected in translocation events. The application of 25 μM ATP caused a Ca^{2+} wave covering the entire cell (Fig. 2, B and C, third and fourth columns). From these data we conclude that PKCα translocation is able to follow Ca^{2+} signals with small amplitudes, brief lifetimes, and spatial restrictions.

During experimental series in which we stimulated PKCα-EYFP–expressing COS1 cells with various lower ATP concentrations (5–25 μM), we found that ~15% of all COS1 cells gave spatially and temporally very complex responses, such as those exemplified in Fig. 3. Fig. 3 B shows relative fluorescence traces from six ROI pairs outlined in Fig. 3 A. These tracings illustrate very short-lived and highly confined increases in the PKCα-EYFP fluorescence (Fig. 3 B, traces 1–5). The individual "hot spots" were spatially independent of one another, but their activity increased, with a variable delay, after ATP application and ceased after ATP washout (unpublished data). As illustrated in the inset of Fig. 3 A (b), the confocal slice was positioned close to the bottom plasma membrane level of this COS1 cell; thus, we recorded PKCα-EYFP fluorescence close to or at the lower plasma membrane. Therefore, the transient increases in the PKCα-EYFP fluorescence were caused by spatially restricted translocation signals to the plasma membrane (local translocation events [LTEs]). LTEs were not restricted to the bottom plasma membrane; similar signals could also be observed at the upper plasma membrane (unpublished data). The detection of LTEs failed either when we increased the ATP concentration or when we moved the confocal section more toward the central region of the cell (unpublished data). Such a loss was not caused by the temporal resolution of our confocal microscope because with charge-coupled device camera–based fluorescence acquisition we do not miss individual events; instead, they might only be blurred over time. Once a cell like the one displayed in Fig. 3 was found repetitive, stimulations with the same ATP concentration after 10–15-min resting periods evoked similar LTE patterns, although not all LTE locations could be restimulated and new ones were additionally triggered during the second ATP stimulation (Fig. 3 C).

In the following, we analyzed a larger population of LTE sites and signals ($n = 160$ from 60 locations; 18 cells). The results of this analysis are shown in Fig. 4. The distribution of the normalized occurrences of spatial spread (Fig. 4 A), lifetime (Fig. 4 B), and amplitude (Fig. 4 C) have been plotted. From these data, it becomes evident that for all of the parameters analyzed the LTEs can be subdivided into two populations.

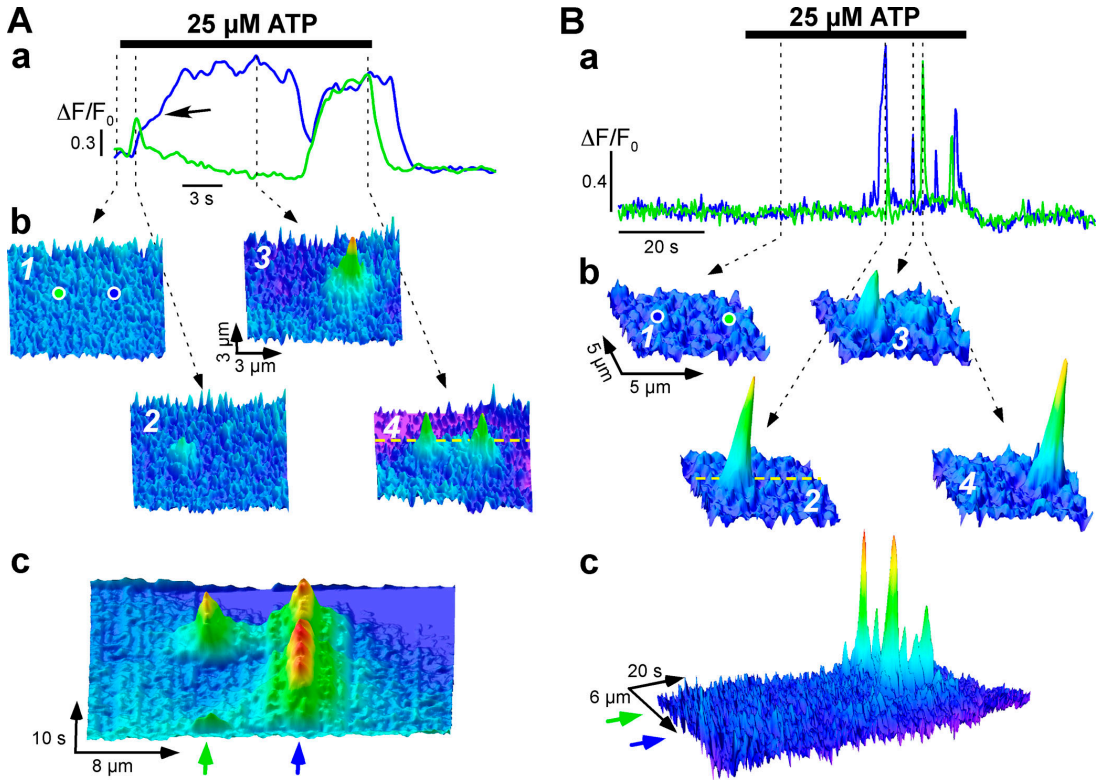

Figure 5. **Spatiotemporal properties of LTEs in COS1 cells.** (A) LTEs in a single PKCα-EYFP–transfected cell after stimulation with ATP. (A, a) The time course of the relative fluorescence signals at the two LTE sites plotted in blue and green, respectively. For selected time points (marked by the vertical dashed lines in a), 3D surface plots of the fluorescence distribution have been redrawn in A b. (A, b 1) indicates the positioning of the two ROIs from which the fluorescence was averaged (traces in A, a). The dashed yellow line in A, b 4 marks the line across the two LTEs used for constructing the 3D surface pseudolinescan image displayed in A, c. Here, time runs into the paper plane, the preserved spatial dimension is represented in the horizontal direction, and the relative fluorescence has been coded in both the color and the height of the 3D surface. The green and blue arrows identify the two LTEs analyzed in A, a. For B, we analyzed two LTE sites exhibiting short-lived LTE signals. The arrangement of B is similar to the one in A. For B c, a linescan image was constructed from lines acquired across the two LTE sites marked with the dashed line in B b 2. Here, time runs from left to right, and the preserved spatial dimension goes into the paper plane.

To investigate the relationship between these parameters, we plotted the amplitude of the LTEs against their individual lifetime (Fig. 4 D). From this graph the following major findings were identified: (a) long and small events were absent, (b) the amplitudes of LTEs did not exceed 150% above resting values, and (c) the two LTE populations found in the individual distributions were also found in Fig. 4 D.

To visualize the spatiotemporal properties of these two populations of translocation signals, we plotted typical LTEs with long lifetimes (>6 s; Fig. 5 A and Video 3, available at http://www.jcb.org/cgi/content/full/jcb.200604033/DC1) and shorter durations (Fig. 5 B). Fig. 5 A exemplifies two LTEs in close spatial proximity (Fig. 5 A, b). Despite continuous ATP stimulation, LTEs can display rather complex time courses (Fig. 5 A). For four selected time points, the PKCα-EYFP fluorescence distributions were plotted as 3D surface plots in Fig. 5 A (b). The 3D surface representation of a pseudolinescan (Fig. 5 A, c) revealed that the spatial spread appears to be functionally limited, as depicted for the long-lasting LTE (black arrow). After an initial 3-s growth period, the spatial spread came to a

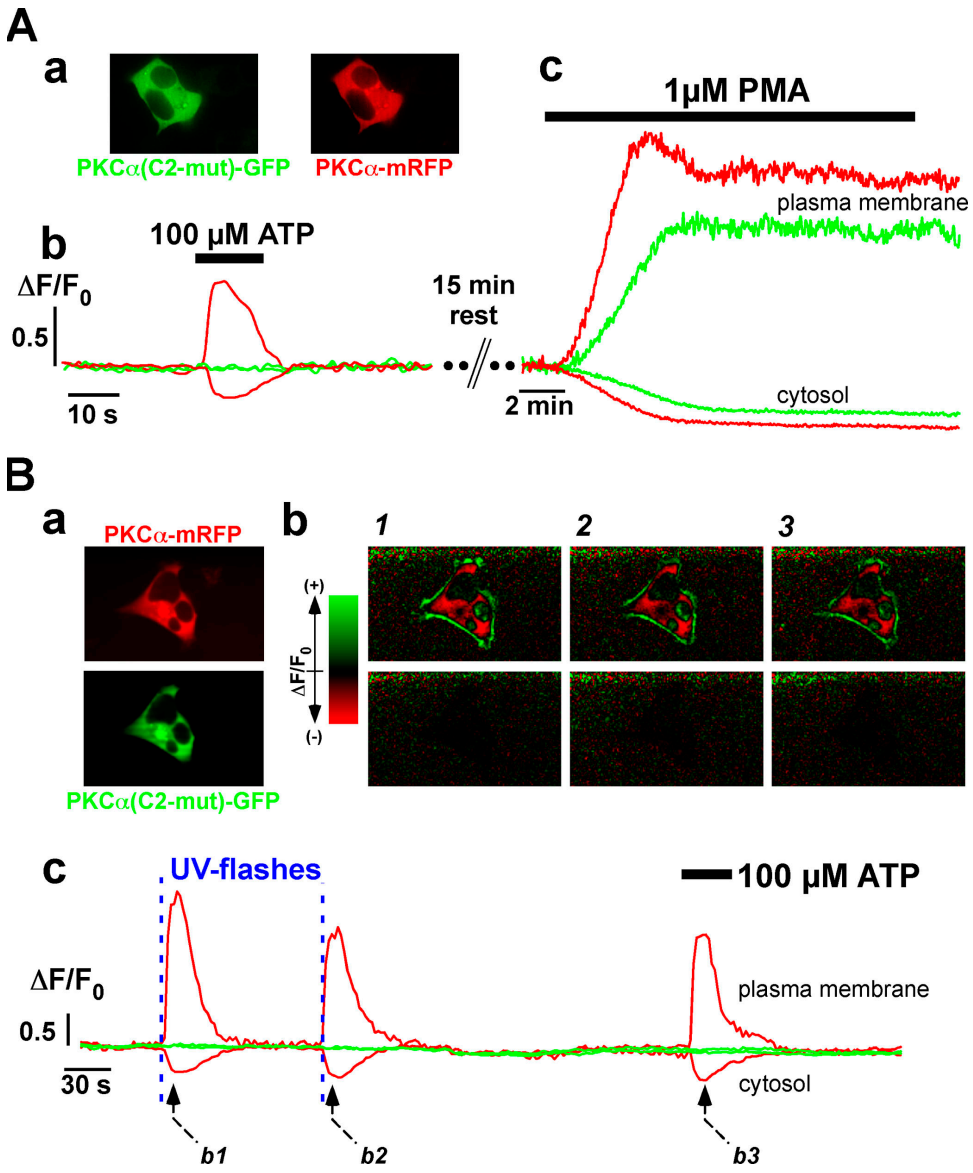

Figure 6. **Role of the C2 domain on translocation properties of PKCα.** HEK293 cells were cotransfected with plasmids coding for PKCα(C2-mut)-EGFP and PKCα(WT)-mRFP. (A) Depicts results in cells stimulated with 100 μM ATP (A, b) and 1 μM PMA (A, c). Green (EGFP fusion protein) and red (mRFP fusion protein) traces depict the time course of fluorescence derived from the plasma membrane (top traces) and cytosol (bottom traces) during the stimulation regimes. Similar results were obtained in 16 independent experiments (n = 51 cells). (B) Translocation responses of WT and C2-mutated PKCs to flash photolytic increases in Ca^{2+}. Cells were loaded with caged Ca^{2+} NPEGTA-AM. B (a) depicts the resting fluorescence of the two PKC constructs, as indicated. B (c) shows the time course of the plasma membrane (top traces) and cytosolic (bottom traces) fluorescence changes of the EGFP construct containing the mutated C2 domain (green) and the WT-mRFP (red). The time points of the UV flashes are indicated by the two blue vertical dashed lines. For the three time points depicted in B (c) by the dashed black arrows, the relative changes of the fluorescence have been replotted in B (b). The color-coded images (see color wedge attached) for the WT (top row) and mutated PKC (bottom traces) are shown. Similar results were obtained in 14 independent experiments (n = 33 cells).

standstill, despite ongoing translocation activity. This finding was typical for all long-lasting LTEs we investigated. From these findings, and from those in Fig. 4 (i.e., two populations of LTEs), we conclude that long-lasting LTEs are characterized by limited amplitudes and spatial spreads.

The C2 domain of cPKC is supposed to mediate the Ca^{2+}-dependent portion of the cPKC membrane interaction (Medkova and Cho, 1998; Verdaguer et al., 1999), whereas the C1a and C1b domains are thought to be responsible for DAG and PMA binding, respectively (Medkova and Cho, 1999; Ananthanarayanan et al., 2003). To investigate the contributions of the C2 or the C1a domains to the translocation of cPKCs and their membrane interactions, we have constructed two PKCα-EGFP fusion proteins lacking a functional C2 and a C1a domain. Fig. 6 depicts results obtained with the wild-type (WT) PKCα-mRFP and the C2-mutated (C2-mut) PKCα-EGFP fusion protein. Although the distribution of the two constructs in resting cells was indistinguishable (Fig. 6 A, a), the ATP stimulation revealed protein translocation only for the WT construct (Fig. 6 A, b; PMA provoked translocation of both proteins). Thus, the mutation we have introduced into the C2 domain specifically suppressed the ATP-induced, but not the PMA-induced, translocation. Because ATP application leads to the generation of two second messengers that interact with the cPKC, i.e., Ca^{2+} (C2 domain) and DAG (C1a domain), we designed experiments that allowed us to distinguish between these two remaining possible membrane interactions. For Fig. 6 B, HEK293 cells coexpressing the two fusion protein constructs were loaded with NP-EGTA–AM, which is a membrane-permeable caged Ca^{2+}. Upon a bright UV flash, NP-EGTA rapidly releases Ca^{2+} (DelPrincipe et al., 1999) and, thus, specifically generates Ca^{2+} signals while avoiding the production of DAG. Two UV flashes in succession triggered the translocation of the WT protein to the plasma membrane (Fig. 6 B, c, red traces; compare top images in Fig. 6 B, b 1 and b 2), whereas the C2-mutated cPKC did not display any change in its subcellular distribution (Fig. 6 B, c, green traces; compare also the bottom images in Fig. 6 B, b 1 and b 2). The ATP application at the end confirmed the translocation properties already described for Fig. 6 A.

For the aforementioned LTEs with lifetimes of <1 s, the translocation speed of cPKC fluorescence proteins has to be very fast. In Fig. 7, we addressed the question of how fast the translocation of the PKCα fusion proteins is in response to a stepwise increase in the intracellular Ca^{2+} concentration. Cells were coloaded with NP-EGTA and fluo-4, and a series of four consecutive UV flashes was delivered. The first two flashes induced only small step changes in the Ca^{2+} concentration (Fig. 7 A, a and b), causing no apparent or only a minute (second flash) translocation of the PKCα construct. Flashes 3 and 4 triggered substantial increases in the intracellular Ca^{2+} concentration that were accompanied by rapid translocations toward the plasma membrane (Fig. 7 B, a and b). To characterize the speed of translocation, we analyzed consecutive images acquired with a frequency of 4 frame pairs/s. Fig. 7 C (2–5) depicts individual images of the fluo-4 ratio (left) and the relative differential changes in the PKCα-mRFP fluorescence (right) before (Fig. 7 C, 2) and directly after the fourth UV flash (Fig. 7 C, 3–5; note that both the fluo-4 and mRPF images were normalized to pre–fourth UV flash fluorescence intensity). Within <250 ms, the cPKC fusion proteins accumulated at the plasma membrane level (see the green outline of the cell in the Fig. 7 C, 3, right). The Ca^{2+} concentration had increased in a stepwise manner and remained constant from Fig. 7 C, 3–5 (left column). From this, we concluded that (a) cPKC translocation required a certain threshold Ca^{2+} concentration and (b) that cPKC translocation to the plasma membrane can occur within <250 ms. Thus, cPKC translocation to the plasma membranes appeared fast enough for the LTEs recorded, but is the dissociation of the cPKC–membrane interaction also fast enough to cause the fast relaxation seen for the LTEs? What contribution do the

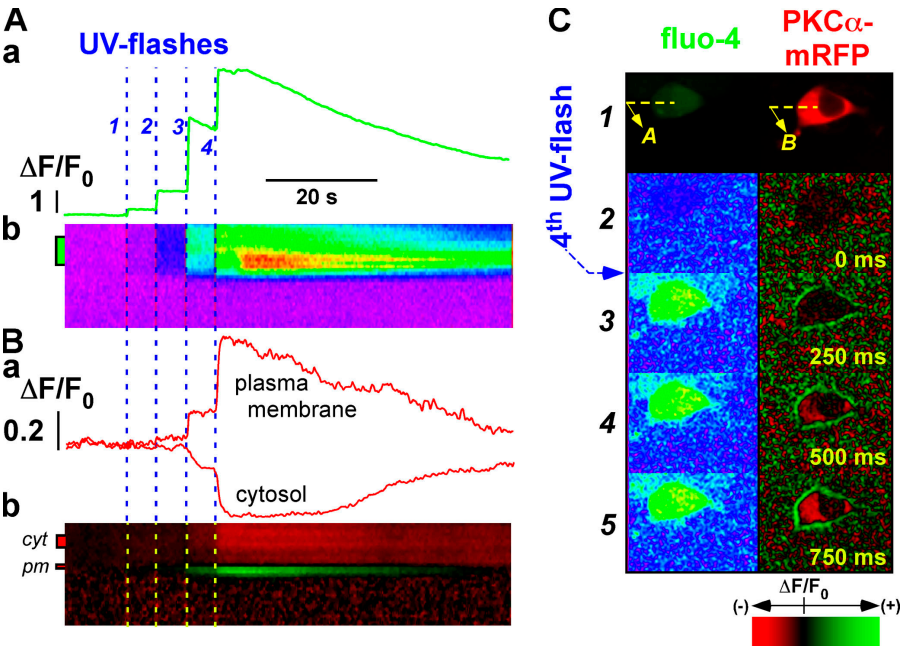

Figure 7. **Recruitment of PKCα to the plasma membrane is very fast.** HEK293 cells were expressing PKCα-mRFP and loaded with fluo-4–AM and NPEGTA-AM. The left part of the figure depicts pseudolinescan images and derived line traces for the fluo-4 fluorescence (A) and PKCα-mRFP fluorescence (B). Four consecutive UV flashes were applied, as indicated by the blue and yellow vertical dashed lines. The regions used for generating the line tracings are marked left of the linescan images. C illustrates exemplified images of the fluo-4 (left) and mRFP (right) fluorescence. The row labeled with 1 depicts the resting fluorescence and the two lines used to generate the pseudolinescan images in A and B (dashed lines). Images in row 2 were taken immediately before the fourth UV flash, and the images in rows 3–5 were obtained at the time points indicated. The fluo-4 and the mRPF images were ratioed against the fluorescence just before the fourth UV flash. The color coding for the mRFP self-ratio images and the mRFP-derived pseudo linescan images in A is shown at the bottom of C. Similar results were obtained in nine additional cells recorded under similar experimental conditions.

C2 and C1a domains make to the membrane residence time or dissociation kinetics?

To address these questions, we expressed WT PKCα-EGFP and coloaded the cells with Fura red and diazo-2, which is a caged Ca^{2+} buffer (Lipp et al., 1996). For these experiments, we restricted the UV illumination during the UV flash to only part of the field of view to simultaneously record cellular responses with and without the UV flash. For the cell depicted in Fig. 8 A (b), we applied a UV flash ∼10 s into the ATP stimulation. This caused a rapid release of a high-affinity Ca^{2+} buffer (K_d = 73 nM) and, consequently, the Ca^{2+} concentration quickly dropped to resting values (Fig. 8 A, b, red trace and Fig. 8 A, d). After this, the cytosolic PKCα-EGFP fluorescence increased (Fig. 8 A, b, black trace), whereas the fluorescence at the plasma membrane level decreased (Fig. 8 A, b, green trace). In Fig. 8 A (b), the black and orange arrows point to a fast and slow component of this decline, respectively. The transition between these two phases was present in all cells analyzed with the same experimental regime (15 cells in five independent experiments), but the fractional contribution of each phase to the total PKCα dissociation process varied between 30 and 60%. From these experiments and from the two populations of LETs we concluded that, indeed, these two time constants of membrane dissociation represent two PKCα pools at the plasma membrane: (a) Ca^{2+}-C2–bound PKCα causing the fast component (Fig. 8 A, b, black arrow) and (b) binding of PKCα via its Ca^{2+}-C2 and DAG-C1 domains causing the second, slower component (Fig. 8 A, b, orange arrow). C1 domain–mediated membrane interactions are much more stable and have a longer lifetime (according to in vitro data; Bittova et al., 2001). To test this hypothesis, we characterized the effect of a functional C1a mutation on the dissociation kinetics of PKCα from the plasma membrane (Fig. 8 B).

For this, HEK293 cells expressing C1a-mutated PKCα-EGFP were loaded with Fura red and diazo-2. The basic experimental design was the same as described for Fig. 8 A. Stimulation of the cells with 100 μM ATP resulted in a robust and reversible translocation to the plasma membrane without apparent differences to the WT construct (compare Fig. 8 A, c, and B, c). Illumination of the cells with a UV flash caused a rapid drop in the intracellular Ca^{2+} concentration (Fig. 8 B, b, red trace) that induced an increase in the cytosolic PKCα(C1a-mut)-EGFP fluorescence back to prestimulation levels (Fig. 8 B, b, black trace). When we analyzed the time course of membrane fluorescence, we found that the fluorescence decay after the UV illumination was only monophasic (Fig. 8 B, b, black arrow), the kinetics of which was similar to the kinetics of the fast component of the WT PKCα (compare green traces in Fig. 8 A, b, and B, b). This lack of a slower decay phase constant was a consistent finding in all cells expressing the mutated cPKC (n = 7 cells in four independent experiments). From this we conclude that the slower dissociation time constant seen in the cells expressing the WT PKCα-EGFP was most likely caused by C1a-mediated membrane interactions, whereas the faster decay was dependent on a functional C2 domain in the protein (Fig. 8 B, d).

Discussion

Signaling cascades using the stimulation of PLCβ result in the production of the $InsP_3$ and DAG that activate $InsP_3$ receptors and PKCs, respectively, with Ca^{2+} release from the ER triggered by $InsP_3$. A tight coupling between intracellular Ca^{2+} signals and PKCα translocation was proposed recently (Mogami et al., 2003). By using the physiological agonist ATP and flash photolysis of caged compounds, we were not only able to provide strong supporting evidence for such an idea but also revealed various pools of PKCα at the plasma membrane. Our findings suggest fast and tight mechanisms for decoding incoming stimuli into translocation signals. Nevertheless, the molecular mass of conventional PKCs (PKCα, ∼82 kD) gives rise to principle doubts as to whether such a protein will be able to follow very fast and brief Ca^{2+} signals (lifetime, <1 s) observed during cellular Ca^{2+} signaling. Although the fluorescence tags of the PKC constructs added another 27 kD to the molecule's molecular mass, the Stokes radius of the fluorescent PKCα only increased slightly (from 42 to 46 Å; Schaefer et al., 2001).

We showed that fluorescent PKCα fusion proteins display graded translocations, which are similar to those reported for glucose stimulation and PKCβ (Pinton et al., 2002). Further establishment of such a notion appears important in the context of PKC-mediated signal transduction because interpretation of amplitudes adds a new dimension to the parameter space that cPKCs can exploit and cells can use to decode incoming stimuli. A similar ability in decoding Ca^{2+} signals has been suggested for calmodulin (Frey et al., 2000).

Cells do not only use the frequency and amplitude domains to decode incoming stimuli into cellular responses, but spatiotemporally complex Ca^{2+} signals have also been described, ranging from global Ca^{2+} waves to spatially restricted Ca^{2+} waves and elementary Ca^{2+} signals, such as Ca^{2+} sparks and Ca^{2+} puffs (for review see Berridge et al., 2000). The importance of such complex signaling processes for cellular signal transduction has been suggested only in an indirect way, by linking local Ca^{2+} signaling to cellular responses or by electrophysiological measurements that allow direct readouts of, e.g., Ca^{2+}-dependent membrane ion conductance in smooth muscle cells (Nelson et al., 1995; Bolton et al., 1999). Nevertheless, it appears important to present direct evidence and visualization of spatiotemporally very complex processes linking local Ca^{2+} signaling to other signal transduction mechanisms. We provide such evidence in that the Ca^{2+} signaling toolbox, from waves to spatially restricted Ca^{2+} signals and elementary Ca^{2+} release events, can indeed be decoded into PKCα translocations to the plasma membrane. Assuming similar properties for all cPKCs, it appears feasible to extend such behavior to the entire cPKC subfamily. An important requirement for such mechanisms is a rapid translocation, despite the substantial molecular mass of our constructs (∼119 kD). With real-time imaging of PKCα translocations after UV flash–induced Ca^{2+} increases, we demonstrated sufficiently fast translocations kinetics (Fig. 7).

It should be noted that not every elementary Ca^{2+} signal will necessarily result in local cPKC translocation because the k_{on} and k_{off} rates of Ca^{2+} binding are very fast, and translocation

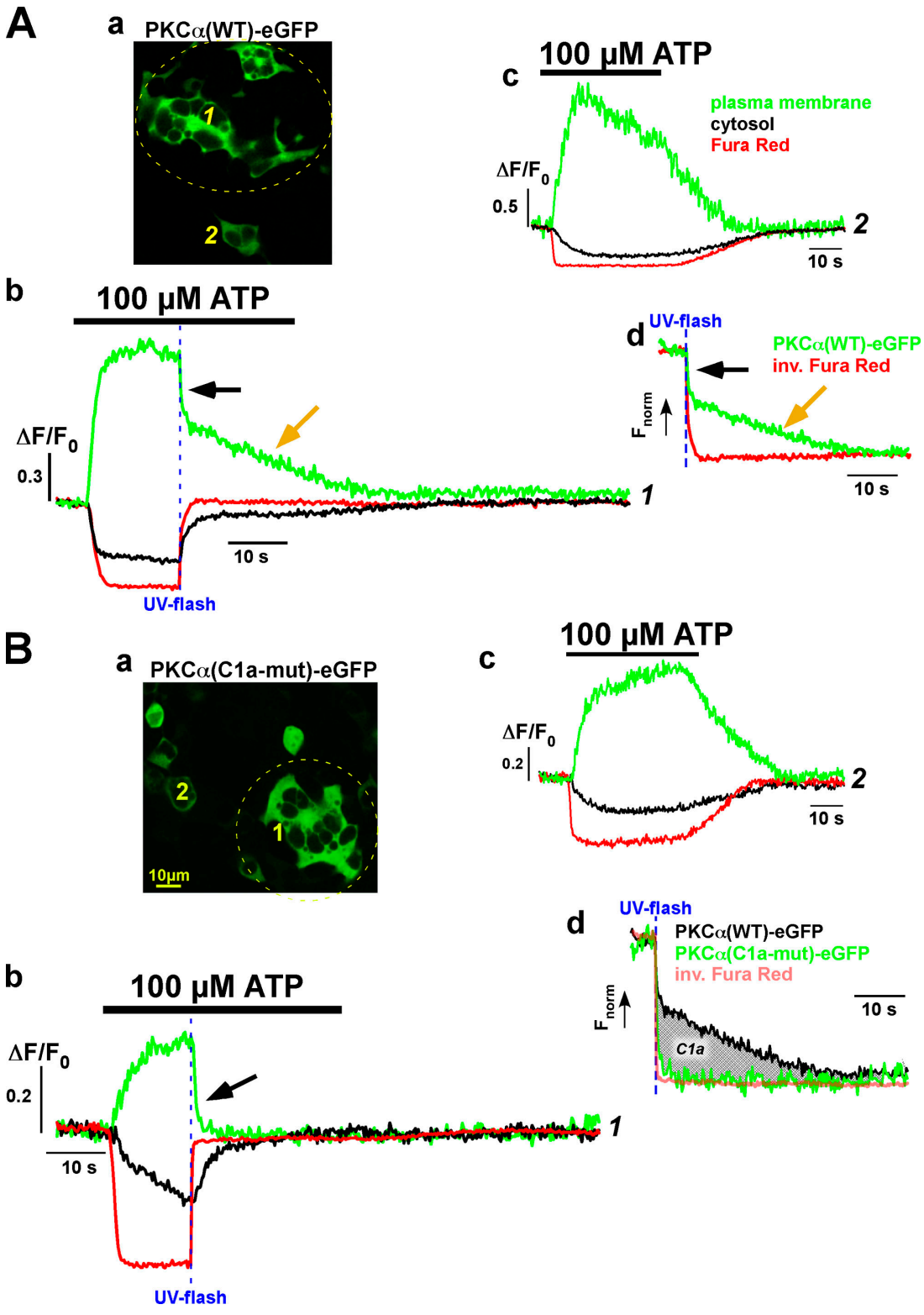

Figure 8. **Contribution of C2 and C1a domains to the PKCα membrane interaction and membrane residence times.** HEK293 cells were expressing PKCα(WT)-EYFP (A) and PKCα(C1a-mut)-EGFP (B) and loaded with Fura red and diazo-2. (A) Fura red and the PKCα(WT)-EYFP fluorescence. The color coding for the tracings is depicted in Ac and the numbers at the traces in Ab and Ac correspond to the cells labeled in Aa. At the time indicated by the vertical dashed blue line in Ab, a UV flash was applied to the area indicated by the dashed yellow circle in Aa. Ac illustrates the behavior of a cell outside of the UV illumination, whereas Ab shows the fluorescence time course of a cell within the illumination area. The black and the orange arrows mark the rapid and slow decay of the plasma membrane fluorescence, respectively. Similar data were obtained in five independent experiments (n = 14 cells). (B) b and c exemplify cells in and out of the UV illumination marked in Ba (dashed circle), respectively. The black arrow in Bb marks the rapid decay of the plasma membrane EGFP fluorescence upon flash-photolytic rapid decrease of the Ca^{2+} concentration. We have overlaid the membrane fluorescence from A (b) and B (b) and the Fura red fluorescence inverted (B, b) in Bd to emphasize the different time courses. The crosshatched area in B (d) illustrates the differences in the time course after C1a mutation. Similar results were recorded in four independent experiments (n = 7 cells).

also requires a certain Ca^{2+} threshold concentration. Ca^{2+} release deeper in the cell will lead to cPKC Ca^{2+} binding, but unbinding of the ion will occur before the cPKC can reach the membrane and encounter PSs and DAG. Thus, only peripheral Ca^{2+} signals or, in other words, only the peripheral component of Ca^{2+} signals, will lead to a significant cPKC translocation. Thus, this is another example of the versatility of Ca^{2+} signals solely depending on their particular location inside cells. Although peripheral transients can induce, e.g., phosphorylation of membrane proteins by the PKC-signaling networks, perinuclear Ca^{2+} release events have been suggested to result in specific nuclear Ca^{2+} signals and trigger accompanying Ca^{2+}-dependent transcription events (Lipp et al., 1997).

Although translocation of the cPKC molecule to its target, the plasma membrane, is an important step in the activation mechanism, the question still remains whether translocation itself can, in fact, indicate activation of cPKCs. This might be rather likely for long-lasting Ca^{2+} transients, given the very high DAG affinity of Ca^{2+}-bound cPKC. In this study, we could provide strong direct evidence for a long-lasting membrane interaction of C1a and DAG in living cells; functionally mutating the C1a domain of PKCα rendered the dissociation process very fast (Fig. 8 B, d); thus, C1a-mediated membrane binding of PKCα represents a significant pool of long-lasting PKCα membrane interactions out of which PKCα could have sufficient time to encounter and interact with target proteins and perform phosphorylation.

In contrast, this is not necessarily obvious for short-lived LTEs. If binding of the C1 and C2 domains to the plasma membrane occurs independently (Johnson et al., 2000), and the initial membrane affinity is mainly determined by its membrane C2 interactions, ionic interactions between the Ca^{2+}-occupied C2 domain and PS in the plasma membrane are the next step (Kohout et al., 2002). The C2 membrane interaction provides the first part of the energy necessary for the allosteric release of the pseudosubstrate from the kinase domain (Newton, 2001). These processes have brought the C1 domain into the proximity of the plasma membrane for C1–membrane interactions that are believed to predominantly determine the residence time of the cPKC at the membrane (Bolsover et al., 2003). After C1a–DAG interactions, the pseudosubstrate is released from the kinase domain that is now ready for substrate interactions and phosphorylation of the target proteins (Nishikawa et al., 1997). Despite the fact that this sequence of events is, in principle, agreed on quite widely, some details are still open for discussion and might have to be reinterpreted in light of our findings of very short-lived LTEs and the two pools of PKCα membrane interactions.

If DAG binding of Ca^{2+}-cPKC is, indeed, the principle event linking the cPKC to the membrane, then how does this notion account for the two populations of lifetimes observed in this study? We propose that these distinct lifetimes reflect different states of the cPKC membrane interactions. As we have previously described, rises in the Ca^{2+} concentration usually "precede" cPKC translocation, and very low-amplitude signals are not necessarily translated into translocation events (Figs. 3 and 7), which is indicative of a certain Ca^{2+} threshold concentration necessary for cPKC translocation. In fact, Ca^{2+} binding to the C2 domain displays a surprisingly low affinity (K_d) of ∼35 μM (measured in vitro in the absence of phospholipids; Kohout et al., 2002). Although we have not been able to provide calibrated Ca^{2+} measurements for the experiments in Fig. 7 (resting Ca^{2+} will be influenced by NP-EGTA), it appears feasible to assume that the Ca^{2+} concentrations evoked by UV flash photolysis of NP-EGTA were much lower than the apparent K_d of 35 μM (DelPrincipe et al., 1999).

Therefore, we suggest that the LTEs with the shorter lifetimes reflect pure Ca^{2+}-dependent binding of PKCα to the plasma membrane. With an apparent diffusion coefficient of 4.67×10^{-7} cm^2/s, a cytosolic viscosity of around 2.0–3.2 cP (Mastro et al., 1984; Schaefer et al., 2001), and an average lifetime of the Ca^{2+}–PKCα complex of ∼12–15-ms molecules can only interact with the plasma membrane when Ca^{2+} binding occurs ≤1 μm away from the plasma membrane (for an illustration see Fig. S2). Furthermore, even for long-lasting Ca^{2+} increases, slower and longer lasting membrane interactions solely driven by Ca^{2+} increases have been described at the global cellular level (Lenz et al., 2002; Sakai *et al.*, 1997). When binding of the Ca^{2+}-C2 domain to the PS of the plasma membranes occurs, the lifetime of the Ca^{2+}-binding complex increases fivefold and, thus, plasma membrane interaction times are significantly prolonged (calculated for PKCα-C2 domain according to in vitro data; Nalefski and Newton, 2001; Kohout et al., 2002; Bolsover et al., 2003). With a putative phosphorylation turnover rate of 380–500 min^{-1} measured in vitro (Sando et al., 1998; Yeh et al., 2002), such brief membrane interactions might, in fact, be sufficient to phosphorylate target proteins in case of an encounter. Elementary Ca^{2+} signals, such as Ca^{2+} puffs, have average lifetimes of ∼1–2 s (Yao et al., 1995; Bootman et al., 1997b; Lipp et al., 1997; Thomas et al., 2000a); thus, the shortest lifetimes of the LTEs observed here are compatible with a purely Ca^{2+}-driven process. This notion is further substantiated in that, upon a stepwise decrease, the Ca^{2+} concentration PKCα(C1a-mut) displayed a rapid membrane dissociation, very closely following the Ca^{2+} decline (Fig. 8 B, d, red transparent trace).

Longer lifetimes of the cPKC membrane complex might indicate additional, and possibly more specific, interactions. Therefore, we propose that the membrane translocations with longer lifetimes represent interactions between the Ca^{2+}-PKCα and DAG. This is particularly interesting because investigation of these lifetimes could yield additional information of that important interaction. Such extended membrane localizations could also indicate additional interactions of the activated cPKCs with receptors of activated kinases (Schechtman and Mochly-Rosen, 2001). Moreover, simultaneous cPKC interactions with several partners will increase the membrane-residence periods overproportionally because redistribution into the cytosol can only occur when the cPKCs unbind from both partners almost simultaneously. Thus, the observed long-lasting translocation events might represent a temporal "walking" of the molecule between dynamic binding/unbinding cycles to the various partners in the plasma membrane. Two additional possible schemes might give rise to such long-lasting translocation events, including highly

repetitive or long-lasting Ca^{2+} puffs, but these can most likely be excluded. Their frequency ought to be well above 2–3 Hz because we have visualized LTEs with lifetimes of around 300–500 ms. Such high-frequency Ca^{2+} puffs have not been imaged yet and are, in fact, rather unlikely taking into account adaptive processes and refractory time periods of the $InsP_3R$ (Berridge et al., 1999). Our experiments (Fig. 8) do not seem to favor the notion of receptor of activated kinase binding because mutation of the C1a domain alone completely suppressed that PKCα pool with the longer membrane-residence time.

On the other hand, long-lasting Ca^{2+} puffs with extended lifetimes (>3–5 s) are also unlikely as the responsible mechanism. Such long-lasting Ca^{2+} puffs have not been described yet, and local depletion mechanisms in the ER might actually terminate local Ca^{2+} release much earlier, as has been proposed for Ca^{2+} sparks (DelPrincipe et al., 1999).

Nevertheless, this cannot easily account for the limited spatial spread of such long-lasting LTEs (Fig. 6 A). For this to occur, at least one of the binding partners has to exhibit a restricted lateral diffusion in the plane of the plasma membrane (∼1 $\mu m^2/s$; unpublished data). The likely candidates for such a mechanism are phosphorylation target proteins that have been anchored in the plasma membrane or membrane lipid domains that were rich in DAG after receptor stimulation. In these situations, residence times of the cPKCs are primarily determined by C1a-DAG binding or target protein interactions in the plasma membrane, and the extent of membrane location will be increased largely.

In conclusion, we propose that the two LTE lifetimes described here represent visual correlates of distinct states of cPKCs during their activation/deactivation cycle. K_{off} rates seem to be predominantly regulating the duration of cPKC membrane interactions with purely C2 domain–dependent membrane interactions being the most dynamic process. C1a domain–mediated membrane or cPKC target protein interactions are more stable, and, consequently, LTEs display a longer lifetime. These notions are supported by our mutation and UV flash experiments, in which we illustrated that C2-mediated membrane interactions were very fast in both directions and that association and dissociation and functional C1a domains largely increased membrane residence times, i.e., decay times were significantly extended. In addition, we provided first evidence that two PKCα populations coexist in the membrane (C2- and C1a-bound proteins), which most likely undergo rapid interconversion.

Our results, thus, foster the understanding of cellular signaling via PKCα (possibly also for the other cPKCs). At resting Ca^{2+} concentrations, the C2 domain repels the PKCα from the membrane because of electrostatic interactions. As soon as the Ca^{2+} concentration is increasing, subplasmamembrane PKCα molecules with a Ca^{2+}-C2 domain bind to the PS in the plasma membrane and the PS–Ca^{2+}–C2 complex is stabilized. Failing to interact with PS causes rapid dissociation from the membrane. This is an essential step that can be imaged as the association of fluorescently tagged PKCα molecules to the membrane. We thus propose that during cellular Ca^{2+} signals Ca^{2+}-C2-PKCα in fact "tiptoes" on the membrane until it "sticks" to a PS. This stabilization step gives the PKCα sufficient time to "probe" for DAG in the membrane. Binding to the DAG (via its C1a domain) further stabilizes the membrane interactions and further increases membrane-residence times. Such a stabilized complex is now given enough time to phosphorylate target proteins.

From this we conclude that, at least for cPKCs, spatial and temporal targeting of cPKC-mediated signaling is mostly, if not solely, driven by the spatiotemporal properties of the underlying Ca^{2+}-signaling machinery.

We believe that these findings put cPKCs in at least the same position as the classic Ca^{2+} signal decoder calmodulin. We have visualized that a downstream signaling molecule, PKCα, is able to decode cellular and subcellular Ca^{2+} signals in all their complexity into translocation and, thus, is an essential linker between Ca^{2+} transients and downstream signal transduction networks (e.g., RhoA, Rac1 or ERK/MAPK; Nakashima, 2002), but also directly phosphorylates membrane proteins such as ion channels and transporters. To our knowledge we illustrated for the first time in living cells that PKCα rapidly converts between various states of membrane interactions and that there are at least two pools of PKCα in the membrane after agonist stimulation.

Materials and methods

Fluorescent PKC fusion proteins

Human PKCα was C-terminally fused to GFP or YFP in a custom-made pcDNA3-EGFP or -EYFP fusion plasmid, as previously described (Schaefer et al., 2001). For the generation of DsRed2 (BD Biosciences) and mRFP (Campbell et al., 2002) fusion proteins, we used pcDNA3-DsRed2 and -mRFP fusion plasmids, respectively.

PKCα mutagenesis

In line with the published results of Medkova and Cho (1998, 1999) on PKCα mutants, we performed site-directed mutagenesis (Kirsch and Joly, 1998) with the primer 5′-TGTTTTGTGGTCCACAAGGCCTGCCATGAATT-TGTTACTTTTTCTTG-3′ in the C1a domain and the primer 5′-CATGAAGTC-ATTCCTTGTCGTACGATCCCAGTTCCAGATTTCTACAGACA-3′ in the C2 domain of the human PKCα-EGFP fusion protein. We generated R77A (PKCα[C1a-mut]-EGFP) to suppress DAG binding to the C1a domain and D246N (PKCα[C2-mut]-EGFP) to suppress Ca^{2+} binding to the C2 domain. All constructs were confirmed by sequencing.

Cell culture and transfection

HEK293 and COS1 (CRL-1573 and CRL-1650; American Type Culture Collection) cells were grown in DME (Invitrogen) supplemented with 5% FBS (PANBiotech), 50 U/ml penicillin, and 50 U/ml streptomycin (both from Invitrogen). Cells were seeded on 20-mm glass coverslips in 12-well plates and transfected the following day at 20–30% confluency with Lipofectamine 2000 (Invitrogen) and appropriate amounts of plasmid DNA per well. All experiments were performed in both cell types and the results shown are representative of both cell types. It must be mentioned that for all the findings we verified in COS and HEK cell lines, we never found qualitative differences between the cell types.

Confocal imaging

Localization and translocation of the fluorescent fusion proteins, as well as changes in the fluorescence of Ca^{2+} indicators such as fluo-4 and Fura red (Invitrogen), were analyzed by laser scanning confocal microscopy. We either used a Nipkow disk–based QLC100 (VisiTech International) equipped with a dual-port adaptor for monitoring two emission wavelengths simultaneously (ORCA-ER cameras; Hamamatsu) or the kilobeam 2D-array scanner–based VTinfinity (VisiTech International) equipped with an ORCA-ER camera for single emission recordings. Both confocal systems were mounted to either an inverted microscope (TE-2000U; Nikon) or an upright microscope (E600; Nikon) and controlled by VoxCellScan software (VisiTech International). Excitation of the fluorescent fusion proteins was performed with the 488-nm line (EGFP or EYFP) or the 568-nm line

(for DsRed2) of an Ar/Kr multiline laser (LaserPhysics). Emission was imaged at wavelengths >500 nm for EGFP and EYFP, and at wavelengths >580 nm for DsRed2. In experiments where we used fusion proteins and Ca^{2+} indicators, we used two different setups. For the first setup, EGFP or EYFP together with Fura red were only excited at 488 nm, while the emissions were imaged at 520 and 600 nm, respectively. For the second setup, fluo-4 and DsRed2 required excitation at two wavelengths (488 and 568 nm), and the emissions were imaged at 520 and 600 nm. Individual images or image pairs were recorded at acquisition speeds ranging from 1 to 10 Hz through 40× (PlanFluor, NA 1.3, DIC H), 60× (PlanApo, NA 1.4, DIC H), or 100× oil immersion objectives (PlanApo, NA 1.4, Ph3 DM; all Nikon). All experiments were performed at room temperature (20–22°C) 2–4 d after transfection. In experiments with Ca^{2+} indicators, the dyes (1 μM fluo-4 AM or 3 μM Fura red AM) were loaded into the cells for 30 min, with an additional 20 min after wash-out for deesterification.

UV flash photolysis of caged compounds

For rapidly increasing or decreasing the intracellular Ca^{2+} concentration, we loaded the cells with 7.5 μM NP-EGTA–AM or diazo-2–AM (Invitrogen), respectively. A UV flash II (Till Photonics) was attached to an upright microscope (E600; Nikon) via an additional epifluorescence input. The UV was directed into the excitation light path via a UV dichroic mirror (HQ450LP; OptiLab). We used a water immersion objective (40×, NA 0.8; Nikon). This allowed for simultaneous recording of the cellular fluorescence and application of the UV flash. The timing between imaging and the flash was programmed within the VoxCellScan confocal software. Because both caged compounds decreased resting Ca^{2+} to an unknown degree, quantitative measurements of Ca^{2+} were not possible. In addition, the amount of Ca^{2+} photoreleased from NP-EGTA largely depends on the amount of (a) photolysed compound and (b) Ca^{2+} loading of NP-EGTA. The latter effect explains the different Ca^{2+} steps in Fig. 8 caused by UV flashes of identical amplitude. Before application of the first flash, the resting Ca^{2+} was very low (K_d for uncaged NP-EGTA 80 nM; upon UV illumination K_d is increased to 1 mM); thus, the amount of photoreleased Ca^{2+} was rather low, but growing with increasing "resting" Ca^{2+} before the subsequent flashes (higher occupancy of NP-EGTA by Ca^{2+}). With AM loading, such effects are largely unavoidable because we could not "preload" the caged compound as is possible when perfusing the cell in the whole-cell configuration of the patch clamp technique used elsewhere (DelPrincipe et al., 1999). Diazo-2 is a caged Ca^{2+} buffer (caged BAPTA) and its K_d is increased upon UV illumination from 2.2 to 73 nM.

Solutions

All experiments were performed in a Hepes (Merck)-buffered salt solution (extracellular medium) composed of (in mM): 135 NaCl, 5.4 KCl, 2 $MgCl_2$, 10 glucose, 2 $CaCl_2$, and 10 Hepes adjusted to pH 7.35 with NaOH. ATP (Sigma-Aldrich) and PMA (Calbiochem) were dissolved as stock solutions in the appropriate solvents and diluted in the external salt solution at the given concentrations before each experiment. Rapid solution switch (exchange time <1 s) was achieved by means of a solenoid-driven custom-made perfusion system. With this system a laminar flow of ~200 μm in diameter was applied to the entire field of view; thus, concentration changes of agonists display global changes occurring simultaneously over the field of view.

Data analysis

After storage of the image, we analyzed the data using ImageJ (W. Rasband, National Institutes of Health, Bethesda, MD). ROI fluorescence over time data were transferred into IGOR software (Wavemerics) and further processed for data display. To account for inhomogeneous dye distribution, we calculated self-ratio images as indicated. For this, we divided subsequent images of a video by a mean image obtained after averaging the 5–10 resting images of each movie (Bootman et al., 1997a,b). Color-coded 2D images were constructed in ImageJ as 8-bit grayscale images to which the given color look-up table was applied. When given in the figures, Ca^{2+} concentrations were calculated as described earlier, assuming a resting concentration of 100 nM (Thomas et al., 2000b). 3D surface representations of individual images or entire movies were calculated with Imaris4 software (Bitplane). All results of our live-cell imaging were analyzed in cells displaying a wide range of expression levels. For the quantitative analysis of LTEs presented in Fig. 4, we had identified criteria that local fluorescence changes had to meet to be treated as LTEs. We identified fluorescence changes as LTEs when their spatial spread was <6 μm, their duration was at least 2 images (or 250 ms) above twofold the standard deviation of the resting signal, and their amplitude was at least two times the standard deviation of the resting fluorescence noise (horizontal dashed line in Fig. 4 D) for at least 2 images (vertical dashed line in Fig. 4 D).

Online supplemental material

Fig. S1 exemplifies HEK and COS cells expressing PKCα fusion proteins showing Ca^{2+} and PKCα oscillations and graded Ca^{2+} and PKCα responses. Fig. S2 shows a model of the mechanisms possibly leading to the generation of LTEs. Video 1 shows the tight relationship between Ca^{2+} oscillations (Fura-Red) and PKCα-EYFP translocation. Video 2 displays the spatiotemporal properties of a PKCα translocation wave propagating through HEK cells stimulated with ATP. Video 3 illustrates the spatiotemporal properties of a long-lasting LTE in COS1 cells upon stimulation with threshold concentrations of ATP. Online supplemental material is available at http://www.jcb.org/cgi/content/full/jcb.200604033/DC1.

We are grateful for the excellent technical support of T. Buhles and A. Vecerdea and for the mechanical engineering of J. Sauerbaum and Dr. K. Neumann. We would also like to express gratitude to our colleagues Drs. S. Ruppenthal, L. Kästner, and U. Kraushaar for critical reading of several versions of this manuscript.

This work was supported by the Deutsche Forschungsgemeinschaft (SFB530 B6 and HBFG-136-418) and the Medical Faculty Homburg Research Support Program.

Submitted: 28 April 2006
Accepted: 11 July 2006

References

Ananthanarayanan, B., R.V. Stahelin, M.A. Digman, and W. Cho. 2003. Activation mechanisms of conventional protein kinase C isoforms are determined by the ligand affinity and conformational flexibility of their C1 domains. *J. Biol. Chem.* 278:46886–46894.

Avkiran, M., and R.S. Haworth. 2003. Regulatory effects of G protein-coupled receptors on cardiac sarcolemmal Na+/H+ exchanger activity: signalling and significance. *Cardiovasc. Res.* 57:942–952.

Berridge, M.J. 2002. The endoplasmic reticulum: a multifunctional signaling organelle. *Cell Calcium*. 32:235–249.

Berridge, M., P. Lipp, and M. Bootman. 1999. Calcium signalling. *Curr. Biol.* 9:R157–R159.

Berridge, M.J., P. Lipp, and M.D. Bootman. 2000. The versatility and universality of calcium signalling. *Nat. Rev. Mol. Cell Biol.* 1:11–21.

Berridge, M.J., M.D. Bootman, and H.L. Roderick. 2003. Calcium: Calcium signalling: dynamics, homeostasis and remodelling. *Nat. Rev. Mol. Cell Biol.* 4:517–529.

Bittova, L., R.V. Stahelin, and W. Cho. 2001. Roles of ionic residues of the C1 domain in protein kinase C-alpha activation and the origin of phosphatidylserine specificity. *J. Biol. Chem.* 276:4218–4226.

Bolsover, S.R., J.C. Gomez-Fernandez, and S. Corbalan-Garcia. 2003. Role of the Ca2+/phosphatidylserine binding region of the C2 domain in the translocation of protein kinase Calpha to the plasma membrane. *J. Biol. Chem.* 278:10282–10290.

Bolton, T.B., S.A. Prestwich, A.V. Zholos, and D.V. Gordienko. 1999. Excitation-contraction coupling in gastrointestinal and other smooth muscles. *Annu. Rev. Physiol.* 61:85–115.

Bootman, M., E. Niggli, M. Berridge, and P. Lipp. 1997a. Imaging the hierarchical Ca2+ signalling system in HeLa cells. *J. Physiol.* 499:307–314.

Bootman, M.D., M.J. Berridge, and P. Lipp. 1997b. Cooking with calcium: the recipes for composing global signals from elementary events. *Cell*. 91:367–373.

Braz, J.C., O.F. Bueno, L.J. De Windt, and J.D. Molkentin. 2002. PKC alpha regulates the hypertrophic growth of cardiomyocytes through extracellular signal-regulated kinase1/2 (ERK1/2). *J. Cell Biol.* 156:905–919.

Campbell, R.E., O. Tour, A.E. Palmer, P.A. Steinbach, G.S. Baird, D.A. Zacharias, and R.Y. Tsien. 2002. A monomeric red fluorescent protein. *Proc. Natl. Acad. Sci. USA*. 99:7877–7882.

Clerk, A., and P.H. Sugden. 2001. Untangling the Web: specific signaling from PKC isoforms to MAPK cascades. *Circ. Res.* 89:847–849.

Codazzi, F., M.N. Teruel, and T. Meyer. 2001. Control of astrocyte Ca(2+) oscillations and waves by oscillating translocation and activation of protein kinase C. *Curr. Biol.* 11:1089–1097.

DelPrincipe, F., M. Egger, and E. Niggli. 1999. Calcium signalling in cardiac muscle: refractoriness revealed by coherent activation. *Nat. Cell Biol.* 1:323–329.

Frey, N., T.A. McKinsey, and E.N. Olson. 2000. Decoding calcium signals involved in cardiac growth and function. *Nat. Med.* 6:1221–1227.

Johnson, J.E., J. Giorgione, and A.C. Newton. 2000. The C1 and C2 domains of protein kinase C are independent membrane targeting modules, with specificity for phosphatidylserine conferred by the C1 domain. *Biochemistry*. 39:11360–11369.

Kirsch, R.D., and E. Joly. 1998. An improved PCR-mutagenesis strategy for two-site mutagenesis or sequence swapping between related genes. *Nucleic Acids Res.* 26:1848–1850.

Kofler, K., M. Erdel, G. Utermann, and G. Baier. 2002. Molecular genetics and structural genomics of the human protein kinase C gene module. *Genome Biol*. 3:RESEARCH0014.

Kohout, S.C., S. Corbalan-Garcia, A. Torrecillas, J.C. Gomez-Fernandez, and J.J. Falke. 2002. C2 domains of protein kinase C isoforms alpha, beta, and gamma: activation parameters and calcium stoichiometries of the membrane-bound state. *Biochemistry*. 41:11411–11424.

Lenz, J.C., H.P. Reusch, N. Albrecht, G. Schultz, and M. Schaefer. 2002. Ca2+-controlled competitive diacylglycerol binding of protein kinase C isoenzymes in living cells. *J. Cell Biol.* 159:291–302.

Lipp, P., C. Luscher, and E. Niggli. 1996. Photolysis of caged compounds characterized by ratiometric confocal microscopy: a new approach to homogeneously control and measure the calcium concentration in cardiac myocytes. *Cell Calcium*. 19:255–266.

Lipp, P., D. Thomas, M.J. Berridge, and M.D. Bootman. 1997. Nuclear calcium signalling by individual cytoplasmic calcium puffs. *EMBO J.* 16:7166–7173.

Manning, G., D.B. Whyte, R. Martinez, T. Hunter, and S. Sudarsanam. 2002. The protein kinase complement of the human genome. *Science*. 298:1912–1934.

Mastro, A.M., M.A. Babich, W.D. Taylor, and A.D. Keith. 1984. Diffusion of a small molecule in the cytoplasm of mammalian cells. *Proc. Natl. Acad. Sci. USA*. 81:3414–3418.

Medkova, M., and W. Cho. 1998. Mutagenesis of the C2 domain of protein kinase C-alpha. Differential roles of Ca2+ ligands and membrane binding residues. *J. Biol. Chem.* 273:17544–17552.

Medkova, M., and W. Cho. 1999. Interplay of C1 and C2 domains of protein kinase C-alpha in its membrane binding and activation. *J. Biol. Chem.* 274:19852–19861.

Mogami, H., H. Zhang, Y. Suzuki, T. Urano, N. Saito, I. Kojima, and O.H. Petersen. 2003. Decoding of short-lived Ca2+ influx signals into long term substrate phosphorylation through activation of two distinct classes of protein kinase C. *J. Biol. Chem.* 278:9896–9904.

Nakashima, S. 2002. Protein kinase C alpha (PKC alpha): regulation and biological function. *J. Biochem. (Tokyo)*. 132:669–675.

Nalefski, E.A., and A.C. Newton. 2001. Membrane binding kinetics of protein kinase C betaII mediated by the C2 domain. *Biochemistry*. 40:13216–13229.

Nelson, M.T., H. Cheng, M. Rubart, L.F. Santana, A.D. Bonev, H.J. Knot, and W.J. Lederer. 1995. Relaxation of arterial smooth muscle by calcium sparks. *Science*. 270:633–637.

Newton, A.C. 2001. Protein kinase C: structural and spatial regulation by phosphorylation, cofactors, and macromolecular interactions. *Chem. Rev.* 101:2353–2364.

Nishikawa, K., A. Toker, F.J. Johannes, Z. Songyang, and L.C. Cantley. 1997. Determination of the specific substrate sequence motifs of protein kinase C isozymes. *J. Biol. Chem.* 272:952–960.

Oancea, E., and T. Meyer. 1998. Protein kinase C as a molecular machine for decoding calcium and diacylglycerol signals. *Cell*. 95:307–318.

Philipson, K.D., and D.A. Nicoll. 2000. Sodium-calcium exchange: a molecular perspective. *Annu. Rev. Physiol.* 62:111–133.

Pinton, P., T. Tsuboi, E.K. Ainscow, T. Pozzan, R. Rizzuto, and G.A. Rutter. 2002. Dynamics of glucose-induced membrane recruitment of protein kinase C beta II in living pancreatic islet beta-cells. *J. Biol. Chem.* 277:37702–37710.

Rettig, J., and E. Neher. 2002. Emerging roles of presynaptic proteins in Ca++-triggered exocytosis. *Science*. 298:781–785.

Sakai, N., K. Sasaki, N. Ikegaki, Y. Shirai, Y. Ono, and N. Saito. 1997. Direct visualization of the translocation of the gamma-subspecies of protein kinase C in living cells using fusion proteins with green fluorescent protein. *J. Cell Biol.* 139:1465–1476.

Sando, J.J., O.I. Chertihin, J.M. Owens, and R.H. Kretsinger. 1998. Contributions to maxima in protein kinase C activation. *J. Biol. Chem.* 273:34022–34027.

Schaefer, M., N. Albrecht, T. Hofmann, T. Gudermann, and G. Schultz. 2001. Diffusion-limited translocation mechanism of protein kinase C isotypes. *FASEB J.* 15:1634–1636.

Schechtman, D., and D. Mochly-Rosen. 2001. Adaptor proteins in protein kinase C-mediated signal transduction. *Oncogene*. 20:6339–6347.

Shirai, Y., K. Kashiwagi, K. Yagi, N. Sakai, and N. Saito. 1998. Distinct effects of fatty acids on translocation of gamma- and epsilon-subspecies of protein kinase C. *J. Cell Biol.* 143:511–521.

Thomas, D., P. Lipp, S.C. Tovey, M.J. Berridge, W. Li, R.Y. Tsien, and M.D. Bootman. 2000a. Microscopic properties of elementary Ca2+ release sites in non-excitable cells. *Curr. Biol.* 10:8–15.

Thomas, D., S.C. Tovey, T.J. Collins, M.D. Bootman, M.J. Berridge, and P. Lipp. 2000b. A comparison of fluorescent Ca2+ indicator properties and their use in measuring elementary and global Ca2+ signals. *Cell Calcium*. 28:213–223.

Verdaguer, N., S. Corbalan-Garcia, W.F. Ochoa, I. Fita, and J.C. Gomez-Fernandez. 1999. Ca(2+) bridges the C2 membrane-binding domain of protein kinase Calpha directly to phosphatidylserine. *EMBO J.* 18:6329–6338.

Vetter, S.W., and E. Leclerc. 2003. Novel aspects of calmodulin target recognition and activation. *Eur. J. Biochem.* 270:404–414.

Yao, Y., J. Choi, and I. Parker. 1995. Quantal puffs of intracellular Ca2+ evoked by inositol trisphosphate in *Xenopus* oocytes. *J. Physiol*. 482:533–553.

Yeh, R.H., X. Yan, M. Cammer, A.R. Bresnick, and D.S. Lawrence. 2002. Real time visualization of protein kinase activity in living cells. *J. Biol. Chem*. 277:11527–11532.